J Musculoskelet Neuronal Interact 2019; 19(1):79-93

Journal of Musculoskeletal and Neuronal Interactions JMNI

Original Article

Neuromuscular dysfunction, independent of gait dysfunction, modulates trabecular bone homeostasis in mice

Steven D. Bain, Philippe Huber, Brandon J. Ausk, Ronald Y. Kwon, Edith M. Gardiner, Sundar Srinivasan, Ted S. Gross

Department of Orthopaedics and Sports Medicine, University of Washington

Abstract

Objectives: To clarify the effects of neuromuscular dysfunction on hindlimb loading, muscle atrophy, and bone homeostasis. **Methods:** We quantified changes to hindlimb loading, muscle atrophy, and bone morphology following either Botulinum toxin A (BTxA) induced muscle paralysis or peripheral nerve injury (PNI) in mice; two *in vivo* models that we anticipated would differently alter gait and mechanical loading patterns due to their distinct effects on neuromuscular signaling. To confirm the expected behavioral effects of PNI, we assessed mechanical allodynia of the ipsilateral hindlimb using von Frey testing and activity (distance traveled and speed) was monitored in both groups using open field testing. Peak vertical ground reaction forces (GRF) and ankle and knee kinematics during normal locomotion were quantified and used to estimate peak mid-diaphyseal normal strains. Muscle atrophy and trabecular and cortical bone morphology were assessed via high-resolution microCT imaging. **Results:** BTxA-induced calf paralysis caused severe muscle atrophy and altered gait kinetics and kinematics and reduced gait-induced normal strains. PNI increased mechanical allodynia but did not alter gait, nor did it cause muscle atrophy. We observed that muscle paralysis and PNI both led to severe trabecular bone loss but only BTxA-induced paralysis increased cortical bone resorption. **Conclusions:** While mechanical stimuli clearly have essential functions in bone development and adaptation, these data emphasize that neuromuscular signaling, independent of load-induced mechanical strains, may modulate trabecular bone homeostasis in normal and disease states.

Keywords: Muscle Atrophy, Bone Homeostasis, Neuromuscular Dysfunction, Neuronal, Adaptation

Introduction

The dependence of bone homeostasis upon normal muscle function is exemplified by the rapid escalation of bone resorption and resulting degradation of bone mass induced by a wide variety of muscle dysfunction pathologies[1-3]. As muscles enable locomotion and functional activity by application of force directly to the skeleton and conditions of muscle dysfunction are associated with diminished skeletal loading, gait-induced bone deformation has been presumed to be the primary means by which normal muscle function maintains bone health[4-8]. In practice, however, it has proven extremely challenging to clarify this relation, as models that alter muscle function (e.g., tenetomy, hindlimb suspension, and sciatic nerve injury) invariably alter gait-induced bone deformation and thus the mechanical environment of bone[9-12].

A number of studies have implemented a recently developed model of transient muscle dysfunction (via a single injection of Botulinum Toxin A; BTxA) to explore muscle-bone interactions in mice[13-16]. Transient muscle paralysis induced by BTxA causes rapid degradation of muscle and vigorous bone resorption (both trabecular and cortical) that is evident at the tissue level prior to muscle atrophy[17,18]. Surprisingly, this tissue degradation occurs coincident with a relatively modest and transient gait deficit[19]. By comparison, maximal trabecular bone loss following hindlimb suspension (which imposes a complete loss of lower limb ground reaction forces), occurs near 4 wk and results in < 50% of the peak loss of trabecular BV/TV following BTxA-induced muscle paralysis[20,21]. Further, while muscle paralysis induces

The authors have no conflict of interest.

Corresponding author: Steven D. Bain, Ph.D., Department of Orthopaedics and Sports Medicine, University of Washington, Box 359798, 325 9th Ave, Seattle, WA 98104
E-mail: sdbain@u.washington.edu

Edited by: G. Lyritis
Accepted 30 October 2018

significant endocortical resorption, hindlimb suspension does not. Given that BTxA is an inhibitor of both motor and sensory neuron function, these data support the thesis that non-mechanical factors emanating from normal muscle function (e.g. intact neuromuscular signaling), may be critical for maintaining bone homeostasis[15].

A role of intact neuromuscular signaling in bone homeostasis is also supported by observations demonstrating that peripheral nerve injury (PNI) results in substantial bone loss. For example, a chronic constriction injury (CCI) of the sciatic nerve in rats caused increased osteoclastic resorption and significantly decreased bone mineral density (BMD) in ipsilateral tibiae[22]. Similar findings have also been observed following partial sciatic nerve ligation (PSN) or spinal nerve ligation (SNL) of L5 and L6 in rats[23]. Interestingly, bone loss following peripheral neuropathy does not appear to be correlated with changes in weight bearing or neuropathic pain behaviors[23]. The potential that non-weight bearing neuromuscular signaling is critical for bone homeostasis is also supported by the extensive recent literature demonstrating that sensory neurons and/or sympathetic innervation can play a direct role in bone homeostasis, as well as muscle derived factors (i.e. myokines), capable of modulating osteoblast and osteoclast function[24-26]. By their potential to act in concert with, or downstream of, gait-induced mechanical loading, these pathways have broadened the context for considering how muscle dysfunction might disrupt bone homeostasis.

In this study, we therefore sought to clarify how neuromuscular dysfunction modulates trabecular and cortical bone homeostasis in mice by assessing gait kinetics and kinematics, muscle volume and bone morphology following BTxA-induced muscle paralysis or peripheral nerve injury (PNI). These *in vivo* models were selected due to the distinct yet overlapping challenges they impose on both hindlimb gait (BTxA-induced paralysis only) and neuromuscular function (BtxA-induced paralysis and PNI)[13,23]. In contrast to the predominant literature in the field, we hypothesized that neuromuscular dysfunction, independent of gait-induced strains, would precipitate trabecular and cortical bone loss. To assess this hypothesis, we quantified peak vertical ground reaction forces (GRF) and ankle and knee kinematics during normal locomotion and used these data to estimate peak mid-diaphysis normal strains. We assessed muscle atrophy and trabecular and cortical bone loss via serial, high-resolution microCT imaging.

Methods

In vivo models

A single injection of Botulinum Toxin A (BTxA; 2 Units/100 g BW; 20 ml injection volume) via Hamilton syringe into the right calf muscle group was used to induce transient muscle paralysis[17,27]. For peripheral nerve injury (PNI), mice were anesthetized with an IP injection of ketamine/xylazine, after which the right sciatic nerve was exposed through a gluteal-splitting approach[28]. Following mobilization of the nerve, a single, 3 mm length of silastic tubing slit longitudinally (Cole-Palmer; ID=0.051 cm; OD=0.094 cm) was placed atraumatically around the nerve. The nerve was then returned to the host bed and the incision was closed with either 5.0 or 6.0 sterile suture as needed. The UW Institutional Animal Care and Use Committee approved both protocols.

Experimental design

Sixteen-week-old C57Bl/6 female mice were randomly assigned to undergo BTxA injection or PNI (n=8 per group). Prior to the intervention, all mice underwent activity monitoring to record locomotor activity, kinetic and kinematic assessment of gait, and microCT imaging as noted below. These data were treated as d 0 baseline data. Subsequently, all data collection was repeated for each mouse on d 5, d 12 and d 28 post-intervention.

Confirmation of mechanical allodynia following peripheral nerve injury

To confirm the expected effect of the PNI procedure, a separate group of 4 female mice (n=4) underwent assessment for mechanical allodynia, which is a behavioral outcome in peripheral neuropathies characterized by increased sensitivity to tactile stimuli[29]. Prior to the experiment, mice were acclimated to the testing apparatus (individual clear Plexiglas boxes on an elevated mesh screen). The mechanical threshold for hindpaw withdrawal was determined by the manual application of calibrated von Frey filaments (weighted nylon fibers applied serially to induce paw withdrawal) to the plantar surface of each hindpaw using the Simplified Up Down Method (SUDO)[30]. Per SUDO, each filament was tested five times per paw, with the mechanical threshold defined as three or more withdrawals out of five trials. Each mouse underwent von Frey testing prior to PNI as a d 0 baseline, and subsequent von Frey assessment on d 5, d 12, and d 28 post PNI.

Activity monitoring

To assess treatment effects on locomotor activity, all mice underwent activity monitoring in an open field testing apparatus (Med Associates, Fairfax, VT). Prior to testing, mice were removed from their home cage and placed in an individual activity chamber and allowed to acclimate in the chamber for 30 minutes. Following acclimation, the computerized video data collection system was activated and the total distance traveled (cm) and average speed (cm/sec) during a 2 hr period was determined for each mouse on d 0, d 5, d 12, and d 28.

Gait dysfunction and quantification of bone strain

We used direct (lower limb kinetics and kinematics) and derived (mid-diaphyseal peak norm strains) outcome measures to assess gait alterations following BTxA-induced

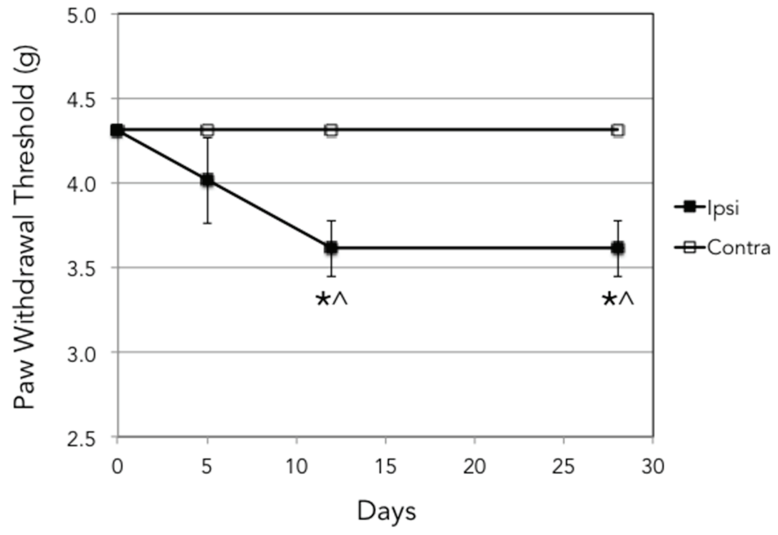

Figure 1. Mechanical allodynia induced by PNI. Mechanical allodynia reached significance (represented by decreased withdrawal threshold) by d12 and was sustained through d 28. No changes in mechanical allodynia were observed in the contralateral limb (*, p<0.01 vs d 0; ^, p <0.01 vs PNI).

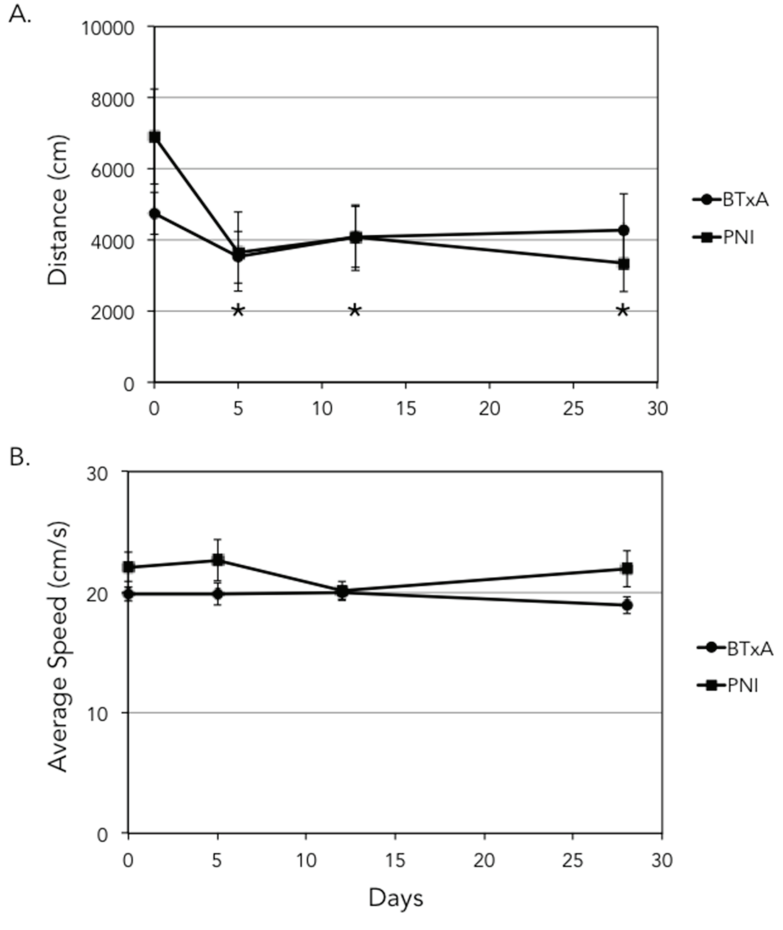

Figure 2. Locomotor activity following BTxA or PNI. The total distance traveled during baseline habituation (d0) was higher in the PNI group vs d 5, d 12, and d 28 (A; (*, p<0.05 vs d 0). There were no significant differences in the BTxA treatment or between groups. There were no differences in average speed at any time point (B).

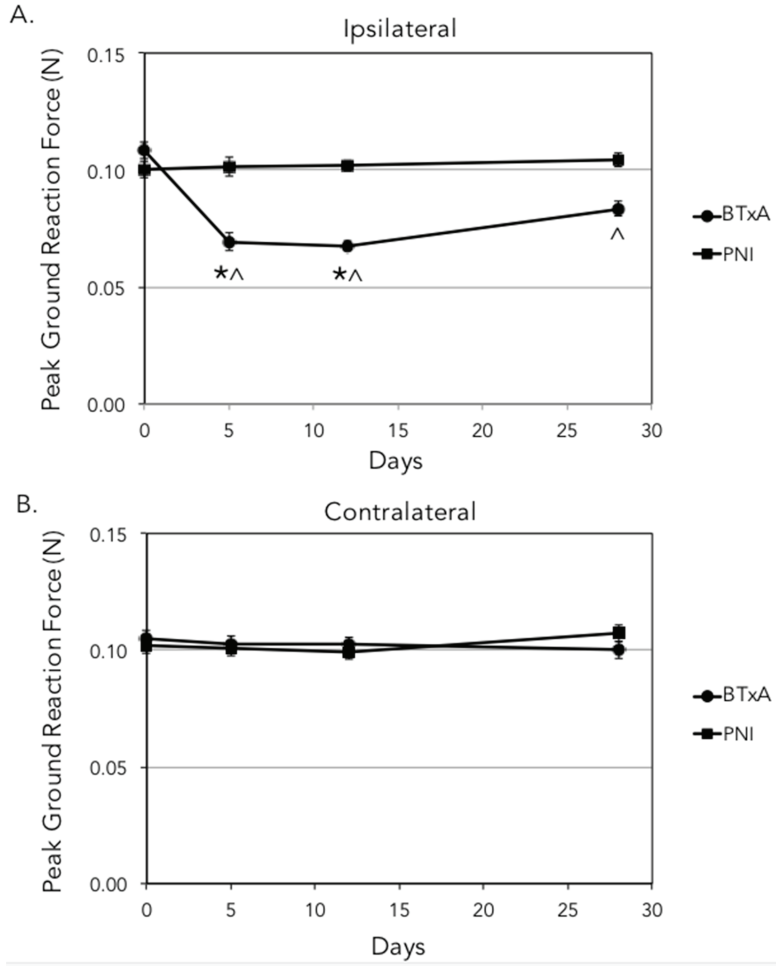

Figure 3. Hind limb ground reaction forces during free ambulation. GRF deficits were observed only following calf paralysis and were confined to the ipsilateral limb (A; *, p<0.01 vs d 0; ^, p <0.01 vs PNI). Contralateral peak vertical GRFs during free locomotion were not altered by either intervention (B).

calf paralysis or PNI. Gait kinetics and kinematics were assessed during free ambulation as each mouse repeatedly walked along an enclosed plexiglas walkway (50 mm wide by 100 mm long) equipped with a miniature force plate (AMTI HE6X, Waterton, MA), centered in the walkway transit. Following acclimation to the testing apparatus, GRFs were collected from force plate contacts with either the left or right hindpaw. Trials were repeated until both left and right hindpaw made clear force plate contact 3 times per leg. Kinematic data for each satisfactory trial was automatically collected when the mouse entered the field of view of a video capture system (Prosilica EC 650C, high speed digital camera, Allied Vision, Exton, PA). Force data were recorded at 200 Hz and video was captured at 30 Hz via customized LabView software.

For each satisfactory walkway transit, ankle and knee kinematics at the time of peak induced vertical GRF were measured using customized LabVIEW software by a single user blinded to the data. For each frame in which the hindpaw was in contact with the force plate, the anatomical relation of the ball of the paw, ankle, knee and hip were digitized and ankle and knee joint angles quantified. Using beam theory, joint angles were used in conjunction with peak GRF to derive peak normal stresses acting at the tibia midshaft. Finally, stresses were converted to strains based on representative tibia mid-shaft geometry (imaged from one of the study mice) and Young's Modulus (E=20 GPa; [31]).

MicroCT imaging

We used high-resolution microCT to quantify cross-sectional muscle volumes and bone morphology following BTxA-induced calf paralysis or PNI. (Scanco μCT40; 10.5 μm voxel size, 55 kVp, 145 μA). While anesthetized with isoflurane, the right hindlimb of each mouse was secured in a custom apparatus and high-resolution images (10 minutes/

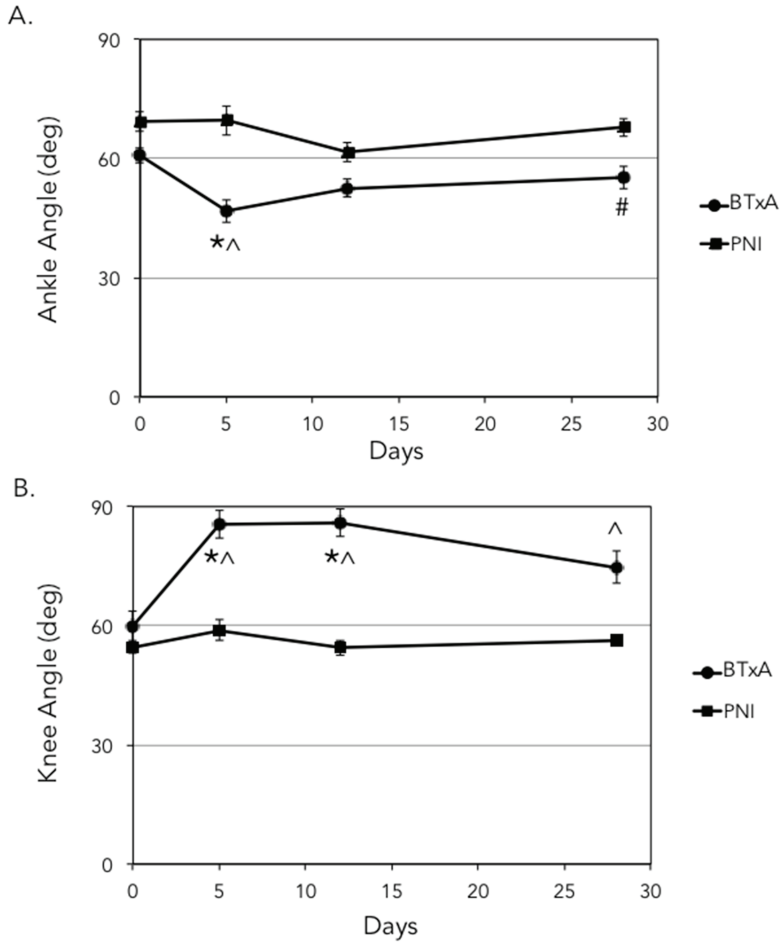

Figure 4. Ankle and knee kinematics during free ambulation. Compared to d 0, calf paralysis decreased ankle flexion at d 5 (A) and increased knee extension at d 5 and d12 during free locomotion (B). Ankle and knee kinematics were not altered vs d 0 in PNI mice (*, $p<0.01$ vs d 0; ^, $p<0.01$ vs PNI; #, $p<0.05$ vs PNI).

scan) were obtained at the right tibia midshaft (2.22 mm long volume initiated 0.65 mm proximal to the tibia-fibula junction) and right proximal tibia metaphysis (2.22 mm long volume initiated at the proximal tibia articulating surface). All raw μCT image data were preprocessed using a Gaussian Filter algorithm to remove image noise (Sigma = 1.2, Support=2.0) followed by bone and muscle segmentation within the scan volume using standard thresholding techniques (a threshold of 720.97 HA/cm^3 was chosen to identify bone tissue; [32]). We quantified lower limb muscle volume (M.Vol) in the mid-shaft scan by determining the total tissue volume (through contour line segmentation of muscle perimeter) and subtracting the periosteal volume of the tibia and fibula within the region. The evaluated region was 1.03 mm long centered within the scan region. We have previously observed that muscle volume changes quantified in this manner are directly correlated with altered calf muscle mass in the model and that calf atrophy accounts for the vast majority of lower limb muscle atrophy (data not shown). We quantified trabecular bone morphology within a 0.86 mm region beginning just distal to the growth plate. Contour lines were applied to the endocortical surface of each slice, then peeled (peel_iter=3) prior to evaluation. We assessed standard trabecular morphology parameters ([32]): Bone Volume (BV), Bone Volume/Tissue Volume (BV/TV), Trabecular number (Tb.N), Trabecular spacing (Tb.S), and Trabecular thickness (Tb.Th). At the mid-shaft, we quantified cortical bone morphology via Periosteal Volume (P.Vol), Endocortical Volume (EC.Vol), Cortical Volume (Ct.Vol) and Cortical Thickness (Ct.Th) through the same volume of interest assessed for muscle adaptation.

Statistics

Repeated measures ANOVAs were performed to assess the main effects of parameter type (BTxA or PNI) and time and their interactions as compared to baseline control values for each

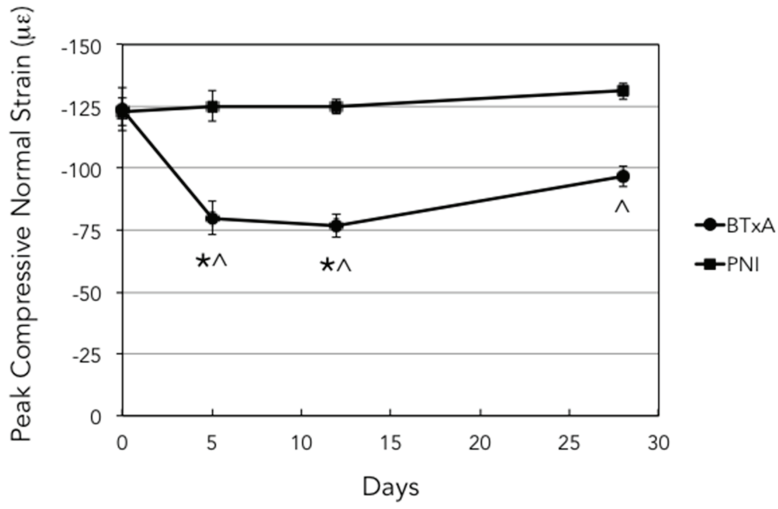

Figure 5. Tibia mid-shaft normal strains at time of peak GRF during free ambulation. Following calf paralysis, peak tibia mid-shaft normal strain was rapidly diminished compared to d 0, but not altered by PNI (*, p<0.01 vs d 0; ^, p <0.01 vs PNI).

main effect. When ANOVA indicated significance, a t-test with Bonferroni correction was performed to identify parameter differences at each time point and parameter differences vs baseline measures (p≤0.05). Single factor linear regression was performed with BV/TV as the dependent variable for either peak strain or muscle volume. Where applicable, all data are expressed as mean values ± SEM.

Results

PNI induced by the placement of a single silastic cuff around the sciatic nerve, led to increased mechanical allodynia of the ipsilateral limb by d 12 (Figure 1), which persisted through d 28. The distance traveled during the baseline habituation period was higher in the PNI group compared to the PNI post-intervention time points at d5 , d 12, and d 28 (Figure 2A). However, there were no differences in distance traveled in the BTxA group at any time point, nor were there any differences between BTxA or PNI. Neither BTxA induced calf paralysis nor PNI altered average speed at any time point (Figure 2B).

With respect to gait analysis, the baseline GRF was equivalent between groups, but the peak GRF of the ipsilateral limb following calf paralysis was significantly reduced at d 5 (Figure 3A; -36.1 ± 3.1 % vs d 0) and d 12 (-36.6 ± 4.5% vs d 0). By d 28, this deficit demonstrated a modest recovery from maximal deficit (+20.5% vs d 5). The decreased GRFs in the ipsilateral limb of the calf paralysis group were also significantly lower compared to the ipsilateral GRFs in the PNI group, which were not significantly altered at any time point. Further, neither BTxA nor PNI altered contralateral peak ground reaction forces (GRF) at any time point, nor were any differences observed between contralateral limbs in the two interventions (Figure 3B).

Calf paralysis transiently altered ipsilateral ankle joint kinematics, as ankle angle was significantly reduced (i.e., less plantarflexion) at d 5 but not at other time points vs d 0 (Figure 4A; -22.8 ± 4.6%; p<0.01). As ipsilateral ankle kinematics following PNI were not altered at any time point, ankle angle following calf paralysis was significantly altered vs PNI at d 5 (p<0.01) and d 28 (p<0.05). BTxA-induced calf paralysis also induced increased knee extension (Figure 4B). Compared to d 0, these kinematic alterations were significant at d 5 (45.6 ± 5.5%, p<0.01) and d12 (48.5 ± 11.2%, p<0.01), but not at d 28 (29.2 ± 11.3%). Compared to the PNI group (no alterations vs d 0), the increased knee extension observed in the calf paralysis group was significant at all time points (p<0.01).

We used peak GRF and joint angles at the time of peak GRF to resolve maximum normal strains acting on the tibia mid-diaphysis during free ambulation. Compared with d 0, BTxA-induced calf paralysis significantly reduced peak normal strain at d 5 and d 12 (Figure 5; -35.4 ± 3.1% and -37.0 ± 3.8%, respectively, p<0.01). At d 28, the decline in peak normal strains was no longer significantly different vs d 0. As PNI did not alter gait induced normal strains, peak normal strains in the BTxA mice were significantly reduced compared to PNI mice at each of the post-intervention time points (p<0.01).

Compared to d 0 muscle volume, atrophy of the lower limb muscle was severe following BTxA injection (Figure 6A), reaching significance by d 5 (Figure 6B; -12.5%, p<0.01), with continued atrophy through d 12 and d 28 (-32.2% ± 0.9% and -41.3% ± 1.3%, respectively, p<0.01). Compared to lower limb muscle volume in the PNI group (which was not altered at any time point), BTxA mice possessed significantly less muscle volume at all time points.

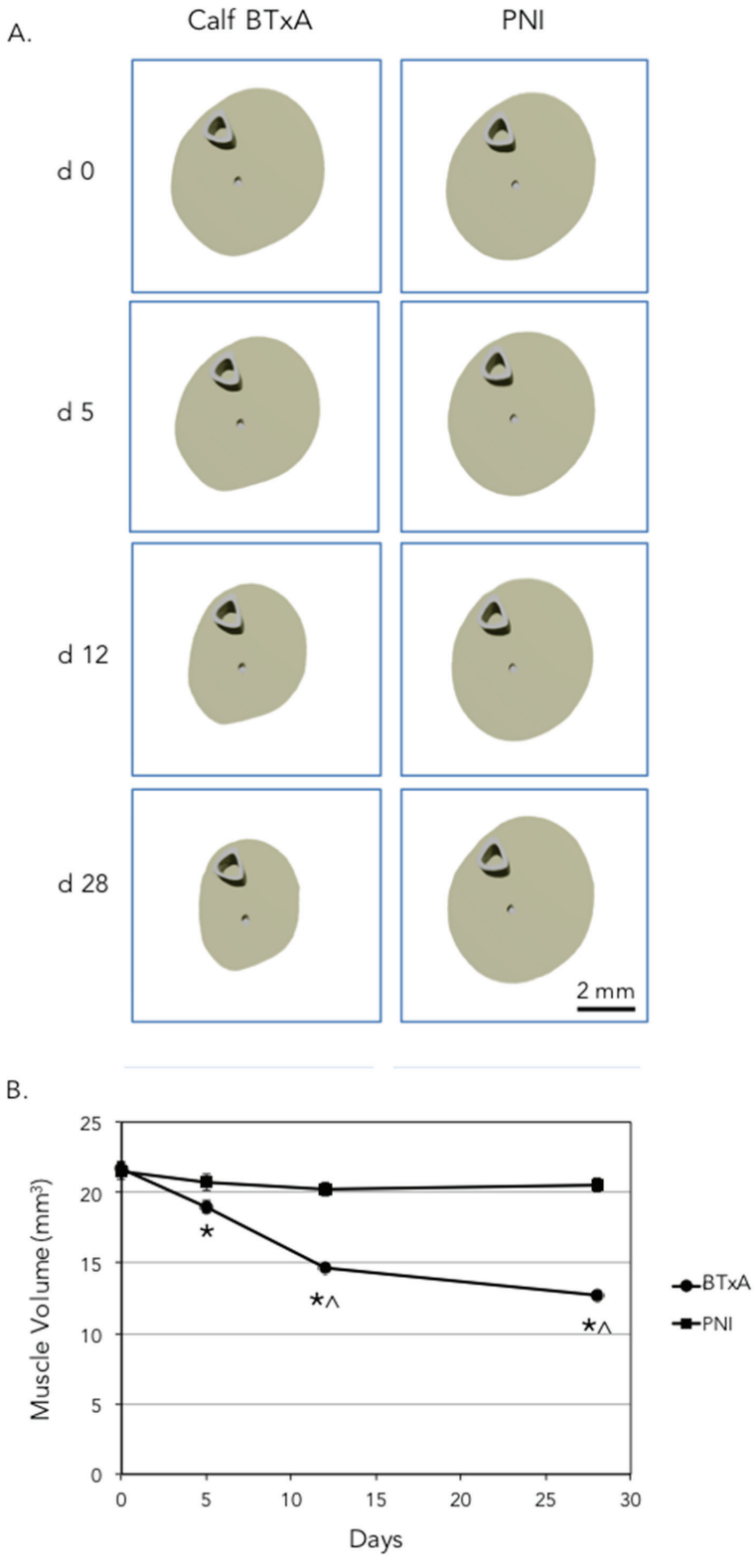

Figure 6. Muscle volume alterations due to BTxA induced paralysis and PNI. Lower limb musculature demonstrated profound atrophy due to calf paralysis (A). Muscle volume was significantly diminished within d 5 of calf paralysis and continued to atrophy through d 28. PNI did not alter muscle volume at any time point (*, $p<0.01$ vs d 0; ^, $p<0.01$ vs PNI).

Table 1. Trabecular and cortical bone morphology derived from microCT imaging.

		d o	d 5	d 12	d 28
Total Volume (mm^3)	BTxA	1.45 ± 0.03 ± % vs do	1.52 ± 0.04* 5.0%	1.59 ± 0.03* 9.7%	1.58 ± 0.03* 9.6%
	PNI	1.49 ± 0.03 ± % vs do	1.54 ± 0.04 3.3%	1.54 ± 0.03 3.7%	1.5 ± 0.02 1.1%
Bone Volume (mm3)	BTxA	0.062 ± 0.004 ± % vs do	0.05 ± 0.003 -18.6%	0.021 ± 0.003*^ -66.2%	0.019 ± 0.001*^ -69.5%
	PNI	0.053 ± 0.002 ± % vs do	0.05 ± 0.003 -4.8%	0.04 ± 0.003* -23.5%	0.035 ± 0.002* -34.5%
BV/TV (%)	BTxA	4.29 ± 0.28 ± % vs d0	3.36 ± 0.29# -21.9%	1.32 ± 0.18* -69.2%	1.19 ± 0.09* -72.4%
	PNI	3.54 ± 0.12 ± % vs do	3.27 ± 0.21 -7.7%	2.61 ± 0.14* -26.4%	2.29 ± 0.14* -35.4%
Total Mineral Density (mg HA/cm^3)	BTxA	1332.8 ± 6.2 ± % vs do	1336.7 ± 5.9 0.29%	1339.8 ± 8.7 0.52%	1339.3 ± 8.6 0.49%
	PNI	1311.9 ± 2.9 ± % vs do	1319.6 ± 3.4 0.59%	1321.2 ± 3.5 0.71%	1330.6 ± 2.6 1.42%
Trabecular Thickness (mm)	BTxA	0.048 ± 0.001 ± % vs do	0.046 ± 0.001 -3.4%	0.038 ± 0.001* -19.6%	0.042 ± 0.001# -11.0%
	PNI	0.045 ± 0.001 ± % vs do	0.043 ± 0.001 -4.9%	0.041 ± 0.001 -8.0%	0.045 ± 0.001 1.3%
Trabecular Spacing (mm)	BTxA	0.42 ± 0.02 ± % vs d0	0.42 ± 0.01 1.1%	0.47 ± 0.02 11.3%	0.49 ± 0.01*^ 18.0%
	PNI	0.41 ± 0.01 ± % vs do	0.42 ± 0.01 0.1%	0.43 ± 0.02 2.7%	0.42 ± 0.02 0.3%
Trabecular Number	BTxA	2.52 ± 0.07 ± % vs do	2.56 ± 0.11 1.7%	2.28 ± 0.1 -9.4%	2.13 ± 0.06* -15.6%
	PNI	2.5 ± 0.06 ± % vs do	2.49 ± 0.07 -0.4%	2.41 ± 0.09 -3.6%	2.53 ± 0.11 1.2%
Periosteal Volume (mm^3)	BTxA	0.96 ± 0.01 ± % vs do	0.95 ± 0.01 -0.7%	0.95 ± 0.01 -1.1%	0.95 ± 0.01 -1.0%
	PNI	0.96 ± 0.01 ± % vs do	0.96 ± 0.01 0.7%	0.97 ± 0.01 1.3%	0.96 ± 0.01 1.0%
Endocortical Volume (mm^3)	BTxA	0.4 ± 0.01 ± % vs do	0.39 ± 0.01 -0.7%	0.43 ± 0.01* 8.4%	0.44 ± 0.01* 12.2%
	BTxA	0.4 ± 0.01 ± % vs do	0.4 ± 0.01 0.0%	0.41 ± 0.01 1.6%	0.41 ± 0.01 2.4%
Cortical Volume (mm^3)	BTxA	0.56 ± 0.01 ± % vs do	0.56 ± 0.01 -0.6%	0.52 ± 0.01*^ -7.8%	0.50 ± 0.01*^ -10.3%
	PNI	0.56 ± 0.01 ± % vs do	0.56 ± 0.01 1.3%	0.56 ± 0.01 1.0%	0.56 ± 0.01 0.0%
Cortical Thickness (mm)	BTxA	0.196 ± 0.003 ± % vs do	0.197 ± 0.003 0.3%	0.179 ± 0.003* -8.5%	0.173 ± 0.004* -11.8%
	PNI	0.193 ± 0.003 ± % vs do	0.196 ± 0.003* 1.2%	0.194 ± 0.004 0.7%	0.193 ± 0.003 -0.1%

*#p < 0.05, *p < 0.01 vs d 0; ^p < 0.01 vs PNI*

As expected, trabecular bone loss following BTxA injection was rapid and severe (Table 1, Figure 7A). BV/TV was significantly reduced vs d 0 at each time point (d 5: -21.4 % ± 5.2; d12: -69.1 ± 3.6%, and d 28: -71.9 ± 2.3%; p<0.01; Figure 7B). Trabecular morphology alterations reflected the profound level of bone loss, with Tb.Th diminished -19.6% and Tb.Sp increased 11.3% at d 12 and Tb.N maximally altered at d 28 (-15.6% vs d0). By d 12, mice exposed to calf paralysis demonstrated significantly reduced trabecular BV (-47.5%), and BV/TV (-49.4%) compared to PNI mice. In contrast, PNI induced steady loss of BV/TV that reached significance at d 12 (-26.1 ± 4.1% vs d 0) and d 28 (-35.0 ± 4.2% vs d 0). PNI only significantly altered Tb.Th at one time point (d12: -8.0% vs d 0) and had no effect upon Tb.Sp or Tb.N.

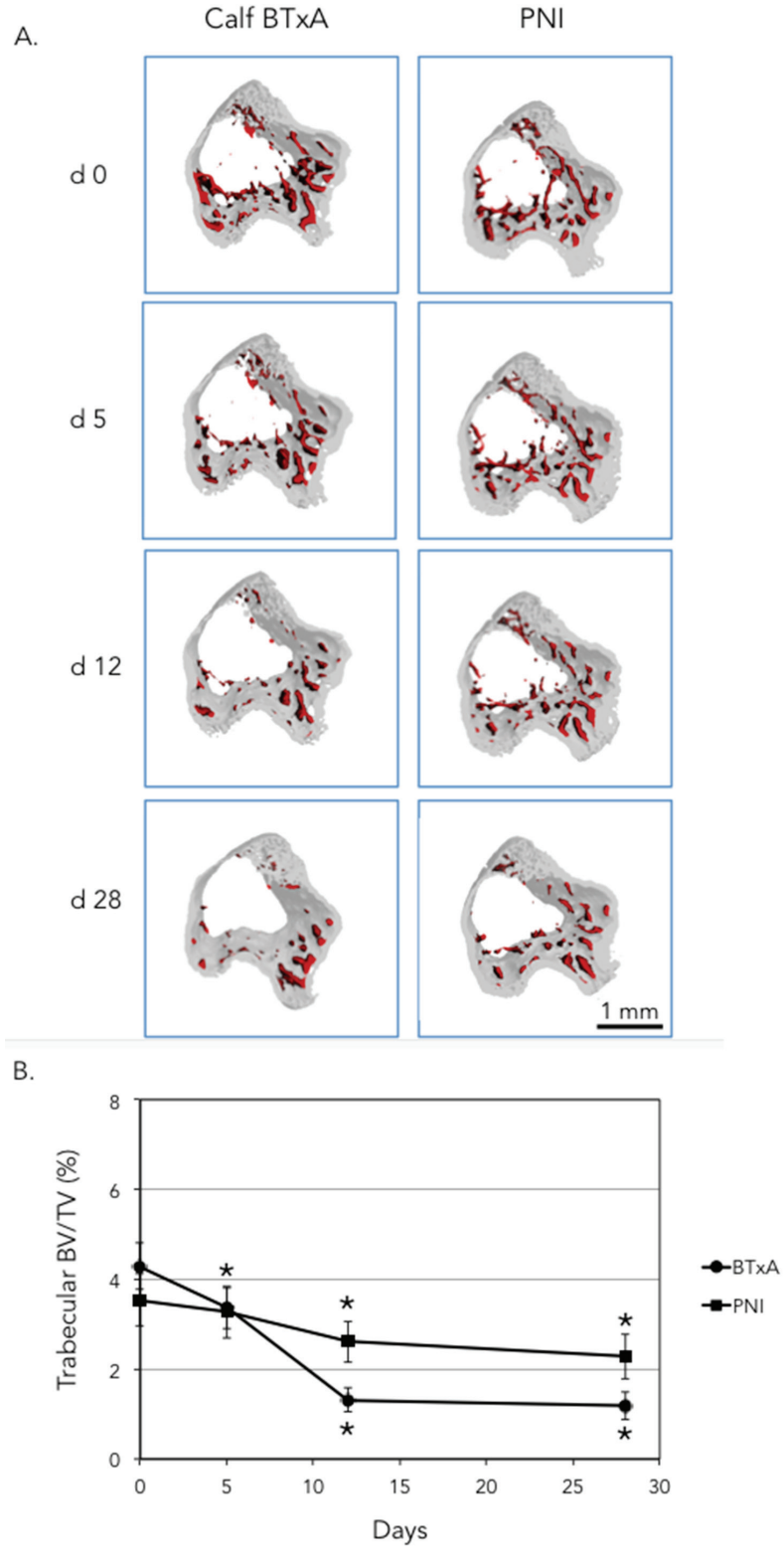

Figure 7. Proximal tibia trabecular bone alterations due to BTxA induced paralysis and PNI. Both calf paralysis and PNI diminished metaphyseal trabecular bone (A, red). Trabecular BV/TV of the proximal tibia metaphysis was significantly diminished by calf paralysis by d 5, while PNI induced bone loss was significant by d 12 (*, $p<0.01$ vs d 0).

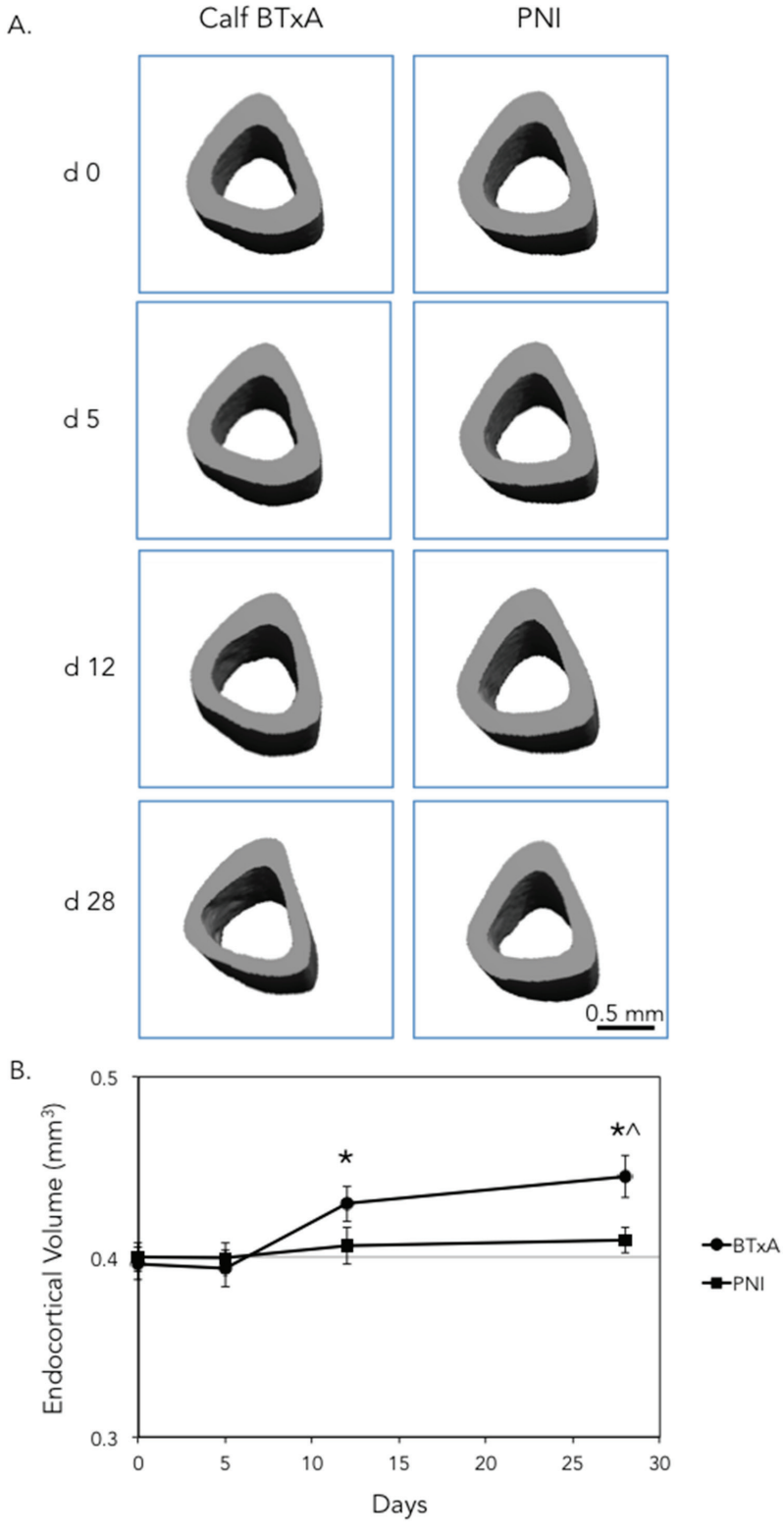

Figure 8. Tibia mid-shaft cortical bone alterations due to BTxA induced paralysis and PNI. Neither intervention altered the tibia mid-shaft P.Vol (A). Calf paralysis resulted in a significant increase in EC.Vol by d 12 that reached 12% by d 28. PNI did not induce significant EC expansion at any time point (*, p<0.01 vs d 0, ^, p <0.01 vs PNI).

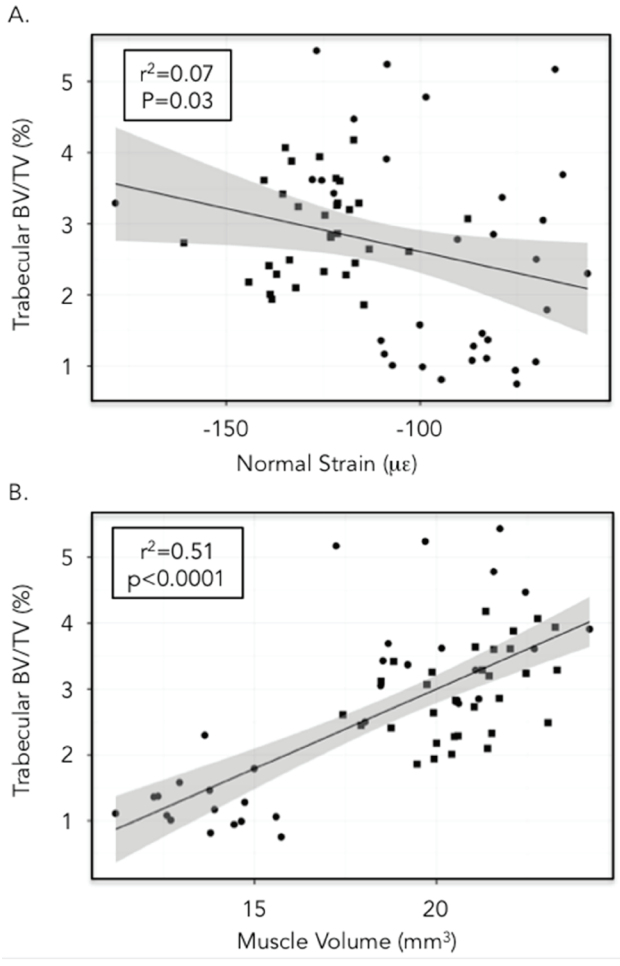

Figure 9. Regression of gait induced normal strain and lower limb muscle volume vs trabecular BV/TV across time points. While normal strain was significantly correlated proximal tibia BV/TV, it only predicted a small portion of the variance of the data (7%; A). In contrast, altered muscle volume predicted 51% of the variability of the BV/TV data (B).

With respect to cortical bone, calf paralysis precipitated a -10.3% loss of cortical bone volume by d 28 ($p<0.01$; Table 1). As periosteal volume was not altered by paralysis, cortical bone loss was achieved entirely by endocortical expansion, which was maximal at d 28 (12.2 ± 1.9% vs d 0, $p<0.01$; Figure 8) and resulted in significantly diminished cortical thickness (d 28: -11.8% vs d0; $p<0.01$). With the exception of a small but significant increase in cortical thickness on d 5 (1.2% vs d 0, $p<0.01$), PNI did not alter any tibia midshaft cortical bone outcome measures at any time point.

Single factor regression analysis across time points revealed that peak normal strain was significantly correlated with metaphyseal BV/TV ($p=0.03$), but only explained 7% of the variation within the data set ($r^2=0.07$; Figure 9A). In contrast, muscle volume was significantly correlated with metaphyseal BV/TV and accounted for 51% of the variation of the BV/TV data ($r^2=0.51$, $p<0.0001$, Figure 9B). With regard to endocortical bone resorption induced in the experiment, normal strain was not significantly correlated with Ec.Vol ($p=0.55$). Muscle volume was, however, significantly correlated with Ec.Vol data ($r^2=0.22$, $p<0.001$).

Discussion

We sought to clarify the impact of neuromuscular dysfunction on trabecular and cortical bone homeostasis. We pursued this goal by assessing gait kinetics and kinematics and muscle and bone atrophy in two *in vivo* models of varied neuromuscular impairment. BTxA-induced calf paralysis led to severe muscle atrophy and precipitated a relatively modest, but significant decrease in gait induced normal strains, and altered ankle and knee kinematics. In contrast, PNI did not alter muscle volume, nor did it significantly alter gait-induced strains, or hindlimb kinematics of the ankle or knee. We observed that BTxA induced alterations to muscle

volume and gait induced strains caused severe trabecular and cortical bone resorption while PNI, which did not alter these parameters, caused significant trabecular bone loss but did not alter cortical bone morphology. In combination, these data provide evidence that intact neuromuscular function, independent of load-induced bone deformations, play an important role in bone homeostasis.

Mechanistically, BTxA and PNI challenge lower limb neuromuscular function in different manners. BTxA inhibits muscular contraction via interruption of acetylcholine transfer at the neuromuscular junction and diminishes afferent sensory signaling[33,34]. BTxA-induced alterations in afferent signaling are sufficient to drive rapid adaptation of the dorsal root ganglia, presumably due to altered neuronal input from distal sites[34]. The combined muscle and neuronal dysfunction resulted in diminished gait kinetics and compensatory lower limb kinematic alterations. In the PNI model, the femoral region of the sciatic nerve was mechanically disturbed throughout the study. This injury leads to axonal degeneration and alters nociceptive signaling with minimal effect on muscle atrophy[28,35]. Consistent with results in similar nerve injury models[23], we did not observe gait dysfunction or loss of muscle volume following PNI. These data, combined with unchanged average speed throughout the experiment, suggest that PNI did not significantly diminish gait-induced mechanical stimuli within the tibia.

BTxA-induced muscle paralysis and PNI also pose differing mechanical and neuromuscular challenges when contrasted with other common musculoskeletal disuse models (e.g., hindlimb suspension, cast immobilization, sciatic neurectomy). In particular, hindlimb suspension (HS) and sciatic neurectomy (SN) provide context for our study. Mechanically, hindlimb suspension causes a complete deprivation of gait-induced kinetics. HS causes muscle specific alterations in acute muscle contraction (increased or decreased, depending on the muscle; [36]) and a shift in fiber type concomitant with muscle atrophy within 2 wk[37]. While these cellular and tissue level alterations require days to weeks to become evident, both transient weightlessness and HS alters sensory afferent signaling within the muscle almost immediately[38,39]. Although PNI did not alter skeletal loading nor muscle volume, the diminished BV/TV in the proximal tibia following HS is nearly identical to that induced by PNI at 2 wk, and, as with PNI, cortical bone is minimally altered by HS[20,21,40]. In contrast, SN decreases peak ipsilateral hindlimb loading similar to that observed following BTxA induced muscle paralysis (approximately -25%; [41]), yet severely degrades trabecular bone and causes significant endocortical resorption[42]. Concomitant with motor and sensory signaling, muscle atrophy is rapid and severe following neurectomy[43]. Thus, our data and the literature clearly highlight the sensitivity of trabecular bone homeostasis to neuromuscular dysfunction. The minimal correlation between diminished mechanical stimuli and trabecular or cortical bone loss observed in our study, while not mechanistic, strongly suggests that intact neuromuscular function, independent of altered mechanical stimuli, is a critical regulator of trabecular homeostasis. Furthermore, the contrasting effects of BTxA-induced muscle paralysis with PNI suggest that cortical bone homeostasis is less sensitive to perturbed neuromuscular signaling.

Although the precise mechanism whereby impaired neuromuscular function initiates rapid trabecular bone loss is not known, we speculate that BTxA-induced calf paralysis and PNI share a common pathway by which dysfunctional neuronal signaling rapidly perturbs trabecular homeostasis. Bone marrow, particularly within the metaphyseal trabecular region, is replete with afferent sensory innervation[44]. Further, it is known that afferent sensory nerves, when provoked by injury, induce an antidromic axonal reflex, which triggers neurogenic inflammation[45,46]. Consistent with this thesis, we have recently reported significant upregulation of the inflammatory cytokines, TNFa and IL-4 within bone marrow 3 d following BTxA-induced paralysis[47]. Neurogenic inflammation, in turn, has potential to mediate osteoclastogenesis and osteoclast function via a variety of inflammatory cells and cytokines[48-52]. Further, this time course is consistent with the onset of RANKL induced osteoclastogenesis that mediates muscle paralysis induced bone loss[18,53]. While speculative, a focal inflammatory response would also provide a rationale for the site specificity of induced resorption by BTxA-induced paralysis[18]. In this context, the more severe the neuromuscular dysfunction (i.e. BTxA > PNI), the greater the neurogenic inflammation, which, in combination with the skeletal loading deficit associated with muscle paralysis, may account for the differential bone loss severity observed following the two conditions.

One general limitation of our study is that while *in vivo* models afford the primary means of exploring how neuromuscular dysfunction impacts connective tissue, it is not possible to completely decouple neuromuscular and mechanical deficits. We attempted to address this limitation via implementation of the PNI model, as the induced neuromuscular dysfunction is less severe than that precipitated by BTxA (with no measureable gait dysfunction and no muscle atrophy). A second limitation of the study is that while altered neuronal signaling with BTxA and PNI has been explored[54-58], we did not directly quantify neuronal dysfunction. Instead, we used muscle atrophy as a surrogate measure of the severity of neuronal dysfunction and confirmed that the nerve cuff model of PNI caused mechanical allodynia[28,59,60]. Additionally, our characterization of altered gait kinetics and kinematics were limited to mid-diaphyseal normal strains during relatively brief activity at specific time points in the study. Thus, these strain data do not represent the complete strain history of the experimental limbs. However, we also assessed 2 hr open-field ambulatory activity across the same time points in this study and (following habituation to the test environment) did not observe any differences in distance traveled or average speed between BTxA and PNI treated mice (all mice demonstrated diminished activity as a function of intersession habituation to the test environment[61,62]). Finally, while we did not detect a

statistical significance between BTxA and PNI induced BV/TV loss, the difference at d 12 (the time of peak BTxA-induced loss) was substantial (-47% vs PNI).

In summary, we observed that a single BTxA injection in the calf muscle group reduced gait kinetics, altered gait kinematics, caused severe muscle atrophy, and precipitated rapid and profound loss of trabecular bone and significant endocortical resorption. PNI, while not altering gait kinetics or kinematics, or causing muscle atrophy, precipitated significant trabecular bone resorption, but did not affect cortical bone. While mechanical stimuli clearly have essential functions in bone development and adaptation, our data emphasize that trabecular bone homeostasis is highly dependent upon muscle health and, in particular, neuromuscular health.

Acknowledgements

The authors thank Dewayne Threet for his efforts in these studies. This work was funded, in part, by NIAMS (AR60304), The Sigvard T. Hansen, Jr. Endowed Chair, and the Zimmer Fracture Biology Professorship.

References

1. Burr DB. Muscle strength, bone mass, and age-related bone loss. J Bone Miner Res 1997;12(10):1547-51.
2. Giangregorio L, McCartney N. Bone loss and muscle atrophy in spinal cord injury: epidemiology, fracture prediction, and rehabilitation strategies. J Spinal Cord Med 2006;29(5):489-500.
3. Gross TS, Poliachik SL, Prasad J, Bain SD. The effect of muscle dysfunction on bone mass and morphology. J Musculoskelet Neuronal Interact 2010;in press.
4. Frost HM. Bone "mass" and the "mechanostat": a proposal. Anat Rec 1987;219(1):1-9.
5. Rubin CT, Lanyon LE. Dynamic strain similarity in vertebrates; an alternative to allometric limb bone scaling. J Theor Biol 1984;107(2):321-7.
6. Slemenda CW, Miller JZ, Hui SL, Reister TK, Johnston CC, Jr. Role of physical activity in the development of skeletal mass in children. J Bone Miner Res 1991;6(11):1227-33.
7. Schipilow JD, Macdonald HM, Liphardt AM, Kan M, Boyd SK. Bone micro-architecture, estimated bone strength, and the muscle-bone interaction in elite athletes: an HR-pQCT study. Bone 2013;56(2):281-9.
8. Macintosh AA, Davies TG, Pinhasi R, Stock JT. Declining tibial curvature parallels approximately 6150 years of decreasing mobility in Central European agriculturalists. Am J Phys Anthropol 2015;157(2):260-75.
9. Wronski TJ, Morey ER. Skeletal abnormalities in rats induced by simulated weightlessness. Metab Bone Dis Relat Res 1982;4(1):69-75.
10. Weinreb M, Rodan GA, Thompson DD. Osteopenia in the immobilized rat hind limb is associated with increased bone resorption and decreased bone formation. Bone 1989;10(3):187-94.
11. Milstead JR, Simske SJ, Bateman TA. Spaceflight and hindlimb suspension disuse models in mice. Biomed Sci Instrum 2004;40:105-10.
12. Brouwers JE, Lambers FM, van Rietbergen B, Ito K, Huiskes R. Comparison of bone loss induced by ovariectomy and neurectomy in rats analyzed by *in vivo* micro-CT. J Orthop Res 2009;27(11):1521-7.
13. Warner SE, Sanford DA, Becker BA, Bain SD, Srinivasan S, Gross TS. Botox induced muscle paralysis rapidly degrades bone. Bone 2006;38(2):257-64.
14. Manske SL, Boyd SK, Zernicke RF. Muscle and bone follow similar temporal patterns of recovery from muscle-induced disuse due to botulinum toxin injection. Bone 2010;46(1):24-31.
15. Warden SJ, Galley MR, Richard JS, George LA, Dirks RC, Guildenbecher EA, Judd AM, Robling AG, Fuchs RK. Reduced gravitational loading does not account for the skeletal effect of botulinum toxin-induced muscle inhibition suggesting a direct effect of muscle on bone [Research Support, N.I.H., Extramural]. Bone 2013;54(1):98-105.
16. Tatara AM, Lipner JH, Das R, Kim HM, Patel N, Ntouvali E, Silva MJ, Thomopoulos S. The role of muscle loading on bone (Re)modeling at the developing enthesis. PLoS One 2014;9(5):e97375.
17. Poliachik SL, Bain SD, Threet D, Huber P, Gross TS. Transient muscle paralysis disrupts bone homeostasis by rapid degradation of bone morphology. Bone 2010;46(1):18-23.
18. Ausk BJ, Huber P, Srinivasan S, Bain SD, Kwon RY, McNamara EA, Poliachik SL, Sybrowsky CL, Gross TS. Metaphyseal and diaphyseal bone loss in the tibia following transient muscle paralysis are spatiotemporally distinct resorption events. Bone 2013;57(2):413-22.
19. Manske SL, Boyd SK, Zernicke RF. Vertical ground reaction forces diminish in mice after botulinum toxin injection. J Biomech 2011;44(4):637-43.
20. Swift JM, Lima F, Macias BR, Allen MR, Greene ES, Shirazi-Fard Y, Kupke JS, Hogan HA, Bloomfield SA. Partial weight bearing does not prevent musculoskeletal losses associated with disuse. Med Sci Sports Exerc 2013;45(11):2052-60.
21. Ellman R, Grasso DJ, van Vliet M, Brooks DJ, Spatz JM, Conlon C, Bouxsein ML. Combined effects of botulinum toxin injection and hind limb unloading on bone and muscle. Calcif Tissue Int 2014;94(3):327-37.
22. Suyama H, Moriwaki K, Niida S, Maehara Y, Kawamoto M, Yuge O. Osteoporosis following chronic constriction injury of sciatic nerve in rats. J Bone Miner Metab 2002;20(2):91-7.
23. Whiteside GT, Boulet JM, Sellers R, Bunton TE, Walker K. Neuropathy-induced osteopenia in rats is not due to a reduction in weight born on the affected limb. Bone 2006;38(3):387-93.
24. Hamrick MW. A role for myokines in muscle-bone interactions [Research Support, N.I.H., Extramural Research Support, U.S. Gov't, Non-P.H.S.Review]. Exerc Sport Sci Rev 2011;39(1):43-7.
25. Johnson RW, White JD, Walker EC, Martin TJ, Sims NA.

Myokines (muscle-derived cytokines and chemokines) including ciliary neurotrophic factor (CNTF) inhibit osteoblast differentiation. Bone 2014;64:47-56.
26. Schnyder S, Handschin C. Skeletal muscle as an endocrine organ: PGC-1alpha, myokines and exercise. Bone 2015;80:115-25.
27. Ausk BJ, Huber P, Poliachik SL, Bain SD, Srinivasan S, Gross TS. Cortical bone resorption following muscle paralysis is spatially heterogeneous. Bone 2012;50(1):14-22.
28. Mosconi T, Kruger L. Fixed-diameter polyethylene cuffs applied to the rat sciatic nerve induce a painful neuropathy: ultrastructural morphometric analysis of axonal alterations [Comparative Study Research Support, U.S. Gov't, P.H.S.]. Pain 1996;64(1):37-57.
29. Colleoni M, Sacerdote P. Murine models of human neuropathic pain. Biochim Biophys Acta 2010; 1802(10):924-33.
30. Bonin RP, Bories C, De Koninck Y. A simplified up-down method (SUDO) for measuring mechanical nociception in rodents using von Frey filaments. Mol Pain 2014;10:26.
31. Akhter MP, Fan Z, Rho JY. Bone intrinsic material properties in three inbred mouse strains. Calcif Tissue Int 2004;75(5):416-20.
32. Bouxsein ML, Boyd SK, Christiansen BA, Guldberg RE, Jepsen KJ, Muller R. Guidelines for assessment of bone microstructure in rodents using micro-computed tomography. J Bone Miner Res 2010;25(7):1468-86.
33. Giladi N. The mechanism of action of botulinum toxin type A in focal dystonia is most probably through its dual effect on efferent (motor) and afferent pathways at the injected site. J Neurol Sci 1997;152(2):132-5.
34. Aoki KR. Review of a proposed mechanism for the antinociceptive action of botulinum toxin type A. Neurotoxicology 2005;26(5):785-93.
35. Balasubramanyan S, Stemkowski PL, Stebbing MJ, Smith PA. Sciatic chronic constriction injury produces cell-type-specific changes in the electrophysiological properties of rat substantia gelatinosa neurons. J Neurophysiol 2006;96(2):579-90.
36. Alford EK, Roy RR, Hodgson JA, Edgerton VR. Electromyography of rat soleus, medial gastrocnemius, and tibialis anterior during hind limb suspension. Exp Neurol 1987;96(3):635-49.
37. Pierno S, Desaphy JF, Liantonio A, De Bellis M, Bianco G, De Luca A, Frigeri A, Nicchia GP, Svelto M, Leoty C, George AL, Jr., Camerino DC. Change of chloride ion channel conductance is an early event of slow-to-fast fibre type transition during unloading-induced muscle disuse. Brain 2002;125(Pt 7):1510-21.
38. Kawano F, Ishihara A, Stevens JL, Wang XD, Ohshima S, Horisaka M, Maeda Y, Nonaka I, Ohira Y. Tension- and afferent input-associated responses of neuromuscular system of rats to hindlimb unloading and/or tenotomy. Am J Physiol Regul Integr Comp Physiol 2004; 287(1):R76-86.
39. Kawano F, Nomura T, Ishihara A, Nonaka I, Ohira Y. Afferent input-associated reduction of muscle activity in microgravity environment. Neuroscience 2002;114(4):1133-8.
40. Judex S, Garman R, Squire M, Busa B, Donahue LR, Rubin C. Genetically linked site-specificity of disuse osteoporosis. J Bone Miner Res 2004;19(4):607-13.
41. Kingery WS, Offley SC, Guo TZ, Davies MF, Clark JD, Jacobs CR. A substance P receptor (NK1) antagonist enhances the widespread osteoporotic effects of sciatic nerve section. Bone 2003;33(6):927-36.
42. Marenzana M, De Souza RL, Chenu C. Blockade of beta-adrenergic signaling does not influence the bone mechano-adaptive response in mice. Bone 2007; 41(2):206-15.
43. Tsai FC, Hsieh MS, Chou CM. Comparison between neurectomy and botulinum toxin A injection for denervated skeletal muscle. J Neurotrauma 2010;27(8):1509-16.
44. Mach DB, Rogers SD, Sabino MC, Luger NM, Schwei MJ, Pomonis JD, Keyser CP, Clohisy DR, Adams DJ, O'Leary P, Mantyh PW. Origins of skeletal pain: sensory and sympathetic innervation of the mouse femur. Neuroscience 2002;113(1):155-66.
45. Foreman JC. Peptides and neurogenic inflammation. Br Med Bull 1987;43(2):386-400.
46. Severini C, Improta G, Falconieri-Erspamer G, Salvadori S, Erspamer V. The tachykinin peptide family. Pharmacol Rev 2002;54(2):285-322.
47. Ausk BJ, Worton LE, Smigiel KS, Kwon RY, Bain SD, Srinivasan S, Gardiner EM, Gross TS. Muscle paralysis induces bone marrow inflammation and predisposition to formation of giant osteoclasts. Am J Physiol Cell Physiol 2017;313(5):C533-C540.
48. White DM. Release of substance P from peripheral sensory nerve terminals. J Peripher Nerv Syst 1997; 2(3):191-201.
49. Fouilloux I, Duplan MB, Baroukh B, Cherruau M, Saffar JL, Lesclous P. Mast cell activation and degranulation occur early during induction of periosteal bone resorption. Bone 2006;38(1):59-66.
50. Lerner UH, Persson E. Osteotropic effects by the neuropeptides calcitonin gene-related peptide, substance P and vasoactive intestinal peptide. J Musculoskelet Neuronal Interact 2008;8(2):154-65.
51. Chiu IM, von Hehn CA, Woolf CJ. Neurogenic inflammation and the peripheral nervous system in host defense and immunopathology. Nat Neurosci 2012;15(8):1063-7.
52. Lewis KM, Turner RJ, Vink R. Blocking neurogenic inflammation for the treatment of acute disorders of the central nervous system. Int J Inflam 2013; 2013:578480.
53. Aliprantis AO, Stolina M, Kostenuik PJ, Poliachik SL, Warner SE, Bain SD, Gross TS. Transient muscle paralysis degrades bone via rapid osteoclastogenesis [Research Support, N.I.H., Extramural Research Support, Non-U.S. Gov't]. FASEB J 2012;26(3):1110-8.
54. Cui M, Khanijou S, Rubino J, Aoki KR. Subcutaneous

administration of botulinum toxin A reduces formalin-induced pain. Pain 2004;107(1-2):125-33.
55. Durham PL, Cady R, Cady R. Regulation of calcitonin gene-related peptide secretion from trigeminal nerve cells by botulinum toxin type A: implications for migraine therapy. Headache 2004;44(1):35-42; discussion 42-3.
56. Ohtori S, Takahashi K, Moriya H, Myers RR. TNF-alpha and TNF-alpha receptor type 1 upregulation in glia and neurons after peripheral nerve injury: studies in murine DRG and spinal cord. Spine (Phila Pa 1976) 2004; 29(10):1082-8.
57. Nakanishi ST, Cope TC, Rich MM, Carrasco DI, Pinter MJ. Regulation of motoneuron excitability via motor endplate acetylcholine receptor activation. J Neurosci 2005;25(9):2226-32.
58. Uceyler N, Tscharke A, Sommer C. Early cytokine gene expression in mouse CNS after peripheral nerve lesion. Neurosci Lett 2008;436(2):259-64.
59. Kraft GH. Fibrillation potential amplitude and muscle atrophy following peripheral nerve injury. Muscle Nerve 1990;13(9):814-21.
60. Hyatt JP, Roy RR, Baldwin KM, Edgerton VR. Nerve activity-independent regulation of skeletal muscle atrophy: role of MyoD and myogenin in satellite cells and myonuclei. Am J Physiol Cell Physiol 2003; 285(5):C1161-73.
61. Tatem KS, Quinn JL, Phadke A, Yu Q, Gordish-Dressman H, Nagaraju K. Behavioral and locomotor measurements using an open field activity monitoring system for skeletal muscle diseases. J Vis Exp 2014;29(91):51785.
62. Bolivar VJ. Intrasession and intersession habituation in mice: from inbred strain variability to linkage analysis. Neurobiol Learn Mem 2009;92(2):206-14.